Polarizabilities of Carbon Nanotubes: Importance of the Crystalline Orbitals Relaxation in Presence of an Electric Field

3 AUTHORS, INCLUDING:

Isabelle Baraille
Université de Pau et des Pays de l'Adour
60 PUBLICATIONS **558** CITATIONS

SEE PROFILE

Michel Rérat
Université de Pau et des Pays de l'Adour
135 PUBLICATIONS **1,918** CITATIONS

SEE PROFILE

Polarizabilities of Carbon Nanotubes: Importance of the Crystalline Orbitals Relaxation in Presence of an Electric Field

DANIEL EHINON, ISABELLE BARAILLE, MICHEL RÉRAT

Institut Pluridisciplinaire de Recherche sur l'Environnement et les Matériaux, UMR C.N.R.S. 5254, Université de Pau et des Pays de l'Adour, Hélioparc Pau-Pyrénées, 2, Avenue du président Pierre Angot, 64053 Pau Cedex 9, France

ABSTRACT: The static polarizabilities of a series of zigzag single walled carbon nanotubes [$(m, 0)$ with $m \neq 3n$ for $m = 7$–25] were computed by the coupled perturbed Kohn-Sham (CPKS) coupled method recently implemented in the periodic CRYSTAL code. This method makes it possible to compute both the longitudinal and transverse polarizabilities with the same approach including the local field depolarization effects for the whole series of the investigated nanotubes. To quantify these effects, the unscreened longitudinal and transverse polarizabilities were also calculated within the linear response theory using the Sum Over States (SOS) method. Our results confirmed the inverse-square dependence on the bandgap of the longitudinal polarizabilities which are found weakly affected by the crystalline orbital relaxation. On the other hand, the comparison between the screened (CPKS) and unscreened (Sum Over States) transverse polarizabilities permit to calibrate more precisely the classical correction of Benedict et al. (Phys Rev B, 1995, 52, 8541) which must be applied to include the local field effect at the SOS level. © 2010 Wiley Periodicals, Inc. Int J Quantum Chem 111: 797–806, 2011

Key words: polarizability; ab initio calculation; nanotube of carbone

1. Introduction

Carbon nanotubes have attracted considerable interest due to their unusual physical prop- erties and great potentials for technological appli- cations including nanoelectronic devices, energy storage, chemical probes, etc. In particular, the response of the carbon nanotubes to electric field was identified as important for a host of potential applications in nanoelectronics [1–3]. Therefore, the static polarizabilities of carbon nanotubes

modeled as periodic systems have been intensively investigated theoretically [4–19]. The most accurate theoretical studies [16–18], which are based on DFT methods calculated the static polarizabilities perpendicular to direction of periodicity (i.e., transverse polarizabilities) numerically through a finite difference method (Finite Field method) to include the local field depolarization effects which is crucial in this direction. As the longitudinal polarizabilities (polarizabilities in the direction of periodicity) are almost unaffected by these effects, they were calculated within the linear response theory using the sum over states (SOS) method which is far less computationally intensive than response polarizabilities obtained through numerical second derivatives. The optical properties of a series of nanotubes were also investigated [20, 21] within density functional theory. The complex dielectric functions were calculated based on the first order time-dependent perturbation theory (similar to the SOS method). These studies did not take the depolarization effect due to the screening of the electric field perpendicular to the nanotube axis into account and did not allow the direct comparison between the calculated transverse dielectric constants and the experimental spectra.

The response to electric field is also important for understanding the gas adsorption on carbon nanotube as Girardet and coworkers showed [22, 23]. In parallel, we developed a new ab initio method to evaluate the long range dispersion coefficient for a molecule adsorbing on a biperiodic system modeling a crystalline surface [24]. The imaginary frequency dependence of the polarizabilities was calculated for each system separately and the dispersion contribution to the interaction potential was evaluated via the Casimir-Polder formula [25]. Our initial objective is to extend this method to the physisorption of small molecules (H_2, N_2, O_2) on the zigzag single walled carbon (m, 0) nanotubes (SWCN) modeled as periodic systems (with nonvanishing gaps for $m \neq 3n$). For that purpose, we need to calculate the dynamic polarizabilities of these nanotubes, within the SOS method and the resulting values must be corrected to include the depolarization effect. This issue can be addressed easily within the classical Clausius Mossotti correction of the unscreened static polarizabilities based on the treatment of the nanotubes as dielectric cylindrical shells of finite thickness [4]. Here, the goal is first to examine the response of zigzag single walled carbon (m, 0) nanotubes with $m \neq 3n$ for

$m = 7$–25 to a uniform external electric field. The coupled perturbed Kohn-Sham (CPKS) method [26, 27] recently implemented in the periodic program package CRYSTAL [28] makes it possible to compute both longitudinal and transverse polarizabilities within the same approach including the local field effect. Then, we can compute the depolarization effects on the whole series of the (m, 0) SWCN, including larger nanotubes than those investigated in previous studies. In particular, we have found new laws over the governing trends for longitudinal polarizabilities. The last goal of this work is to compare the screened (CPKS) and unscreened (SOS) polarizabilities to calibrate more precisely the classical correction of Benedict et al. that we will apply to the calculations of dynamic polarizabilities.

2. Theory and Computational Details

All nanotube geometries were generated by TubeGen [29]. The semiconductors zigzag single walled carbon nanotubes (m, 0) with $m \neq 3n$ for $m = 7$–25 were investigated in this study. All-electron density functional theory (DFT) calculations were performed in the framework of the periodic linear combination of atomic orbitals (LCAO) approximation as implemented in the periodic program package CRYSTAL developed in Torino [28, 30]. The crystalline orbitals are expanded in terms of localized atomic gaussian basis set, in a way similar to the L.C.A.O (Linear Combination of Atomic Orbitals) method currently adopted for molecules. The eigenvalues equations are solved using both the local LDA (local density approximation) approach [31, 32] and the B3LYP hybrid functional based on the Becke's three parameters adiabatic connection exchange functional [33] in combination with the Lee-Yang-Parr's correlation functional [34]. Both LDA and B3LYP approaches were found to give results in agreement with the experimental data for both graphite and graphene. The number of k points in the first irreducible Brillouin zone in which the Hamiltonian matrix is diagonalized is equal to 40. All electron (AE) basis set was used for orbital expansion solving the Kohn-Sham equation iteratively. The carbon atoms were described by a 6-21G* basis set as a compromise between calculation cost and accuracy. This basis is sufficient to give trends in the series of the studied nanotubes. The exponents of the most diffuse shells were optimized

for the graphene sheet: $\xi(sp) = 0.2159$ bohr^{-2} and ξ (d) $= 0.8356$ bohr^{-2} for LDA or $\xi(sp) = 0.2218$ bohr^{-2} and ξ (d) $= 0.8935$ bohr^{-2} for B3LYP. We set the total energy tolerance to 10^{-9} hartree and eigenvalue tolerance to 10^{-8} hartree in the iterative solution of the Kohn-Sham equations. The level of accuracy in evaluating the Coulomb series is controlled by five parameters, for which standard values given in CRYSTAL (i.e. 8 8 8 8 14) have been used.

All calculations reported in this article were carried out using the development version of the CRYSTAL code in which the CPKS method has recently been implemented to compute analytically the response to static fields with periodic boundary conditions [26, 27]. This method includes field-induced orbital relaxation and allows to access reliability and accuracy in the calculation of materials polarizabilities, for ab initio single-determinantal approximations. The CPKS static polarizabilities (α) can be considered as reference values including both major contributions: (i) the noninteracting single-particle excitations which give rise to the unscreened static polarizabilities (α_0) as computed in the SOS method (ii) the interactions between single-particle excitations which make the total field felt by the electrons lower than the externally applied field by producing a depolarization local field. While the Finite Field method [35, 36] evaluates the perturbation of the external electric field (as a "sawtooth" electric potential in the directions of periodicity) by numerical differentiation, the CPKS polarizabilities are calculated by analytical differentiation leading to less time-consuming calculations. In the CPKS method, the relaxation of the crystalline orbitals is taken into account via the calculation of the external electric field perturbed density electronic matrix. As the electronic relaxation is not yet taken into account, the first SCF cycle in the CPKS algorithm corresponds to the SOS method in which only vertical transitions between occupied initial crystalline orbitals $|i\rangle$ and unoccupied $|j\rangle$ crystalline orbitals for a k point in the first Brillouin zone (BZ) are considered, $\Delta\varepsilon_{ij\,\vec{k}} = \varepsilon_{j\vec{k}} - \varepsilon_{i\vec{k}}$ being the corresponding vertical transition energies. Moreover, as the potential part of the Kohn-Sham operator commutes with the electron position operator $\vec{r}$, either the velocity operator ($\vec{\nabla}_{\vec{r}} + i\vec{k}$) used by Gajdos et al [37] or the length operator ($\vec{\Omega}_k = ie^{i\vec{k}\cdot\vec{r}}\vec{\nabla}_k e^{-i\vec{k}\cdot\vec{r}} = \vec{r} + i\vec{\nabla}_k$) can be used within both SOS and CPKS formalisms [38]. In our previous works [39–42], the velocity operator

was preferred for SOS calculations: the transition moments between orthogonal crystalline orbitals are equal to $\langle i|\vec{\nabla}_r|j\rangle_{\vec{k}}/(\varepsilon_{j\vec{k}} - \varepsilon_{i\vec{k}})$, instead of, $\langle i|\vec{r} + i\vec{\nabla}_k|j\rangle_{\vec{k}}$ as if the hypervirial theorem was checked. This latter condition is not satisfied for the Hartree-Fock exchange potential and as a consequence for the hybrid functionals [43]. For a pure DFT Hamiltonian (LDA or GGA), both velocity and length operators must lead to the same values of the CPKS polarizabilities if the basis set of atomic orbitals is complete. The convergence criteria for the CPKS cycle (10^{-4}) is estimated on the polarizability tensor diagonal elements.

The polarizabilities initially computed per unit cell are converted to polarizabilities per unit length to make easier the comparison in the series of the investigated nanotubes. All the polarizabilities reported in the following are in Å^2.

For most crystalline systems, the local field effects represent roughly 10% of the polarizabilities. However, for surfaces, these effects are much greater for the transverse polarizabilities due to the build up of bound surface charge. For the carbon nanotubes, bound charge will build up on the cylindrical surface of the tube and create a local depolarization field. As a result, the unscreened transverse polarizability (α_0^{zz}) is roughly 3–4 time larger greater than the screened one (α^{zz}). Therefore, the SOS transverse polarizabilities (linear response from independent-particle approximation) are usually corrected to estimate the depolarization effect with the classical Clausius Mossotti relation applied to a cylindrical volume ($V = \pi \times \tilde{R}^2 \times L$):

$$\alpha^{zz} = \frac{\alpha_0^{zz}}{1 + \frac{2\alpha_0^{zz}}{\tilde{R}^2}}$$

where $\tilde{R} = R + \delta R$ is the effective radius of the tube, which takes into account the delocalization of the electrons mainly the π electrons that participate to the screening. The adjustable parameter δR represents the radial extension of the π orbitals. On the other hand, because the nanotube is infinitely long, the depolarization field component along the x direction should be tiny, as supposed in previous works [18, 19].

3. Results and Discussion

The aims of this article required two separate analyses according to the direction of the applied

TABLE I

Direct gaps (in eV) of the zigzag single walled carbon (*m*, 0) nanotubes with $m \neq 3n$ for *m* = 7–25: comparison with previously published experimental and theoretical results.

SWNT	Radius (Å)	Exp. [44]	[17,18]	LDA	B3LYP
(7,0)	2.80	1.298	0.398	0.369	1.178
(8,0)	3.19	1.598	0.562	0.499	1.252
(10,0)	3.98	1.073	0.860	0.875	1.191
(11,0)	4.38	1.196	0.815	0.764	1.039
(13,0)	5.17	0.896	0.700	0.697	0.936
(14,0)	5.57	0.957	—	0.609	0.817
(16,0)	6.36	0.764	—	0.574	0.768
(17,0)	6.75	0.799	—	0.507	0.676
(19,0)	7.55	0.664	—	0.485	0.647
(20,0)	7.94	0.686	—	0.435	0.578
(22,0)	8.74	0.587	—	0.420	0.559
(23,0)	9.13	—	—	0.380	0.504
(25,0)	9.93	—	—	0.370	0.491

electric field. Longitudinal and transverse polarizabilities per unit length were calculated within the three approaches finite field (FF), CPKS, and SOS at both LDA and B3LYP levels for the zigzag SWCN (*m*, 0) with $m \neq 3n$ for *m* = 7–25. Both the velocity $(\vec{\nabla}_{\vec{r}} + i\vec{k})$ and the length $(\vec{\Omega}_k = \vec{r} + i\vec{\nabla}_{\vec{k}})$ operators (noted *V* and *L*, respectively) were used for LDA calculations while only the length operator was considered at the B3LYP level. All calculations were carried out of electric dipolar gauge "*U*" and the transition moments were computed by taking into account the same number of virtual orbitals as the valence occupied ones. The CPKS results that include analytically the full response to the electric field are used as reference to analyze and improve the SOS values using the parametrized method derived from the classical Clausius Mossotti relation.

A preliminary analysis of the calculated bandgaps is necessary because of the crucial role the transition energies play in the calculation of the polarizabilities. Experimental and theoretical direct band-gaps of the studied SWCN are listed in Table I. All these systems are found to be semiconductor. Our gap values are in agreement with previous calculations. The LDA values are widely undervalued in comparison with the experimental values reported in the literature [44, 45]. These results are part of the well-known defect of the LDA method, which despite a correct description of the semiconductors electronic structure, systematically underestimates the widths of the band gap, usually by 30–50%. The B3LYP method gives band gaps within 0–15% of

experiment in agreement with the results found with this functional for a wide range of semiconductors and insulators [46].

The longitudinal and transverse components of the polarizability tensor are highly anisotropic, as can be expected from the one-dimensional character of the SWCN. Effectively, the second order perturbation energy, which can be approximated by the SOS formula depends in particular on the transition energies and, then, increases when the gap decreases. This gap decreases with the radius of the tube while the valence and conduction band widths are enlarging. Nevertheless, the transition moments which appear at the numerator of the SOS polarizability are not all allowed at the same resonances according to the field direction. As shown by the data reported in Table II, the highest values of the longitudinal oscillator strengths appear at the smallest transition energies. Here, the (10, 0) and (11, 0) nanotubes have been taken as examples to illustrate a general trend in the whole series. The active transverse transitions are essentially found beyond 10 eV and are lower than the longitudinal ones, making the nanotubes more conductors in the parallel direction, i.e., having a larger SOS polarizability component in this direction. Moreover, as we will see in the next sections, there is no polarization effect along the direction of the nanotube considered as an infinite 1-D system, while the depolarization effect in the perpendicular direction is relatively important leading to a decrease of the perpendicular component of the polarizability.

TABLE II

Transverse (z direction) and longitudinal (x direction) electronic transitions energies (in eV) and oscillator strengths[a] (in a.u.) for the (10,0) and (11,0) nanotubes at the Γ points of the first Brillouin zone in the energy range 0–20 eV. To facilitate the comparison between the two systems, the values f^{xx} and f^{zz} reported in the table correspond to "normalized" oscillator strength: the oscillator strengths have been divided by the total number of electrons per unit cell.

(10,0)				(11,0)			
E (eV)	f^{xx}	E (eV)	f^{zz}	E (eV)	f^{xx}	E (eV)	f^{zz}
0.87	4.04	1.22	0.52	0.76	3.13	0.97	0.49
1.85	1.16	1.50	0.64	1.45	2.47	1.24	0.58
2.52	1.91			2.77	1.67		
3.10	1.60			3.24	1.44		
3.13	1.70			3.29	1.53		
9.86	0.30			3.68	0.38		
9.89	0.32			9.80	0.24		
10.47	0.19	10.48	0.35	10.08	0.34		
10.76	1.01	10.51	0.46	10.33	0.16		
10.88	0.20	10.96	0.35	10.82	0.91		
11.58	0.60	11.16	0.32	10.91	0.28		
12.75	1.27	12.23	0.15	11.50	0.85	11.64	0.16
13.04	1.05	14.63	0.48	12.83	1.09	12.06	0.18
13.59	0.75	14.73	0.63	13.05	1.02	12.50	0.14
14.21	1.04	17.11	0.15	13.22	0.71	14.46	0.59
15.96	0.27	17.55	0.37	13.90	1.00	14.55	0.68
16.24	0.40	17.68	0.19	15.53	0.56	16.61	0.17
17.11	0.28	18.36	0.18	15.72	0.54	17.09	0.23
19.18	0.49			16.80	0.24	17.30	0.33
19.29	0.41			17.45	0.11	17.97	0.20
				17.63	0.11		
				18.19	0.42		
				18.34	0.51		

[a] $f_{ij\,\vec{k}} = (2/3)(\varepsilon_{j\vec{k}} - \varepsilon_{i\vec{k}})\langle i|\vec{\Omega}_k|j\rangle_{\vec{k}}^2$.

3.1. LONGITUDINAL POLARIZABILITIES

The SOS and CPKS longitudinal polarizabilities (α_0^{xx} and α^{xx}, respectively) are reported in Table III. The LDA/CPKS values computed with the length operator (L) are slightly higher (4–5%) than those obtained with velocity operator (V). This weak difference should be due to the non completeness of the atomic orbitals basis set. Note that the effect of the basis set on the quality of the SOS and CPKS results was studied in a previous work [38]. The comparison between the unscreened (SOS) and screened (CPKS) values shows that the local field effect affects only weakly the longitudinal component at the LDA level (less than 2% for the length operator). On the other hand, the depolarization effect is more important at the B3LYP level. The difference between the SOS and

CPKS values decreases from 12% for (7,0) to 4% for (25,0) when the radius of the nanotube increases. The SOS values are systematically lower than the CPKS ones.

The comparison between the longitudinal polarizabilities computed at the B3LYP and LDA levels shows that the latter are on average higher by 28% for CPKS and 38% for SOS from the B3LYP reference. For the SOS approach, these differences decrease from 56% for (7,0) to almost 34% for the nanotubes with the highest radii while they increase slowly from 25% for (8,0) to 28 % for (25,0) for the CPKS method. They can be directly connected to the values of the gaps (E_g). As shown on Figure 1, the relative errors between the two DFT methods (from the B3LYP reference) on the longitudinal polarizabilities compare very well with those calculated on the inverse of the band gap ($1/E_g$), except for the (7,0) and (8,0)

TABLE III

Longitudinal SOS and CPKS polarizabilities per unit length (in Å^2) of the zigzag single walled carbon (m, 0) nanotubes with $m \neq 3n$ for m = 7–25. Both the velocity and the length operators were used for LDA calculations [LDA(V) and LDA(L), respectively] while only the length operator was considered at the B3LYP level [B3LYP(L)].

|	LDA(V)		LDA(L)		B3LYP(L)	
	SOS	CPKS	SOS	CPKS	SOS	CPKS
(7,0)	87.59	86.58	92.75	90.68	59.50	67.87
(8,0)	108.64	108.72	114.14	112.85	80.15	90.14
(10,0)	139.21	139.63	148.91	146.98	106.35	116.53
(11,0)	179.32	181.12	190.70	188.69	137.01	149.04
(13,0)	213.58	216.77	230.34	228.16	168.24	180.71
(14,0)	268.71	274.90	289.21	286.61	212.00	226.51
(16,0)	307.58	316.35	335.11	332.58	246.72	261.29
(17,0)	375.56	390.18	409.89	406.73	303.47	320.59
(19,0)	421.01	439.98	464.94	461.97	343.80	360.97
(20,0)	500.10	529.17	555.07	551.35	413.08	432.93
(22,0)	554.54	590.82	623.15	619.70	462.13	482.06
(23,0)	643.52	695.93	728.91	724.61	544.56	567.26
(25,0)	709.17	773.08	814.20	810.19	604.71	627.49

SWCN. These results confirm the well known gap-dependence of the longitudinal polarizability underlined in previous studies and confirmed by the high values of the oscillator strengths in the energy range around the gap. Notice that, for all the SWCN, almost 50% of the total longitudinal polarizability arise from the low-lying active transitions around the gap while the other 50% come

from higher transitions which are less sensitive to the value of the bandgap.

However, there is still a controversy in the literature about this governing trend. The static longitudinal polarizability is found proportional either to the inverse band gap $1/E_g$ when divided
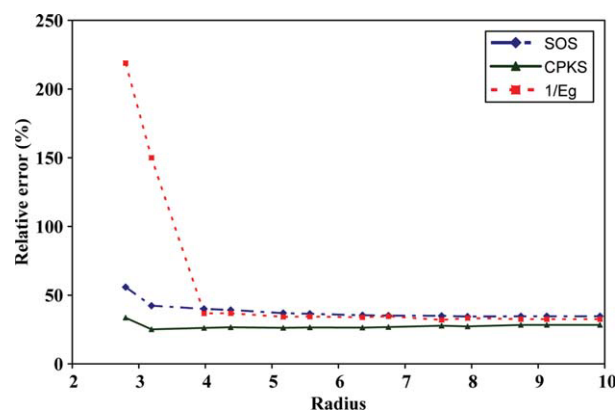
FIGURE 1. Relative errors (in %) between the LDA(L) and B3LYP(L) methods (from the B3LYP reference) on the longitudinal SOS and CPKS polarizabilities and the inverse of the band gap ($1/E_g$) as a function of the SWCN radius (in Å). [Color figure can be viewed in the online issue, which is available at wileyonlinelibrary. com.]
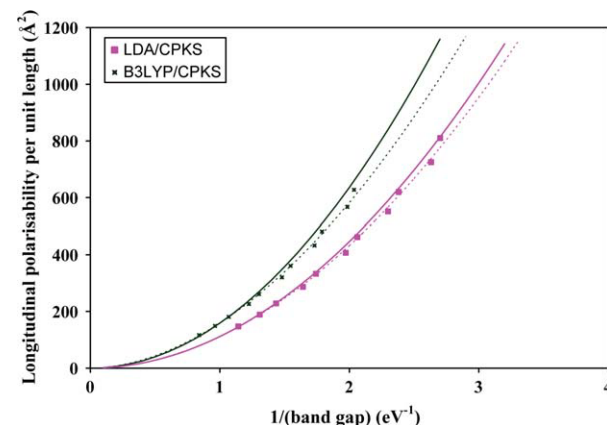
FIGURE 2. CPKS longitudinal polarizabilities per unit length as a function of the inverse band gap at the LDA and B3LYP levels (m = 10–25). The dashed curves correspond to the best less squares fits by $y = ax^\gamma$ type functions (γ = 1.87 or 1.95 at the B3LYP and LDA levels, respectively). The solid curves are $y = ax^2$ parabola with the same constant as the fitted dashed curves. [Color figure can be viewed in the online issue, which is available at wileyonlinelibrary.com.]
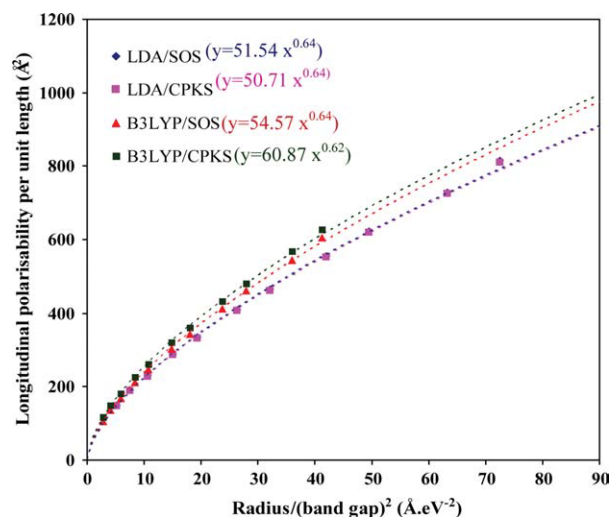
FIGURE 3. Longitudinal polarizabilities per unit length as a function of the radius over band gap squared in both CPKS and SOS approaches at the LDA and B3LYP levels. The four curves have been fitted by $y = ax^\beta$ type functions whose expressions are given in the captions. [Color figure can be viewed in the online issue, which is available at wileyonlinelibrary.com.]

by the number of atoms in the unit cell [18, 19] or to R/E_g^2 when divided by the length of the tube [4, 12]. Our results confirm that there is rather an inverse-square dependence on the gap as shown on Figure 2 for the CPKS longitudinal polarizability per unit length. Nevertheless, the best less squares fits on our longitudinal polarizabilities

per unit length have been obtained on the R/E_g^2 dependence using $y = ax^\beta$ type functions (see Fig. 3). The exponent is found at about $\beta \sim 0.64$ for the four approaches (LDA/CPKS, LDA/SOS, B3LYP/SOS, and B3LYP/CPKS). Only the narrowest (7,0) and (8,0) nanotubes deviate from this general trend as previously underlined by Kozinsky and Marzari [12] who proposed a linear dependence on R/E_g^2 for the series $(m,0)$ with $m = 10$–17. In conclusion, our result show that the longitudinal polarizability of the zigzag SWCN $(m, 0)$ with $m \neq 3n$ for $m = 7$–25 is proportional to R/E_g^2 rather than either $1/E_g^2$ or $1/E_g$.

The application of the FF method to the longitudinal polarizabilities proves to be difficult and time-consuming. Indeed, it seems almost impossible to find a compromise between the applied electric field intensities and the number of unit cell needed to obtain converged values. An extrapolation of the B3LYP/FF longitudinal polarizabilities computed for the (7,0) nanotube allows to estimate the size of the supercell needed to converge on the CPKS value at 22 unit cells (i.e., 616 carbon atoms).
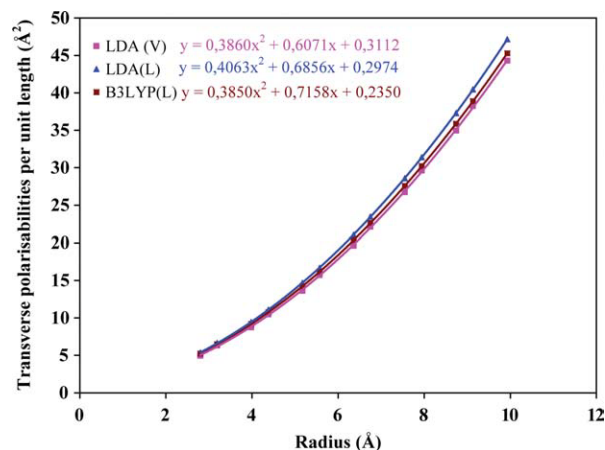
3.2. TRANSVERSE POLARIZABILITIES

The SOS and CPHF(KS) transverse polarizabilities per unit length (α_0^{zz} and α^{zz}, respectively) are reported in Table IV. The FF transverse polarizabilities that are not reported here have been

TABLE IV _____

Transverse SOS and CPKS polarizabilities per unit length (in Å^2) of the zigzag single walled carbon $(m, 0)$ nanotubes with $m \neq 3n$ for $m = 7$–25. Both the velocity and the length operators were used for LDA calculations [LDA(V) and LDA(L), respectively] while only the length operator was considered at the B3LYP level [B3LYP(L)].

	LDA(V)		LDA(L)		B3LYP(L)	
	SOS	CPKS	SOS	CPKS	SOS	CPKS
(7,0)	23.14	4.95	25.61	5.38	19.62	5.24
(8,0)	31.03	6.33	33.22	6.66	25.04	6.47
(10,0)	42.52	8.75	46.64	9.45	35.68	9.18
(11,0)	51.86	10.47	55.85	11.10	42.44	10.75
(13,0)	67.67	13.64	73.98	14.69	56.50	14.22
(14,0)	78.69	15.74	85.00	16.71	64.65	16.15
(16,0)	98.36	19.64	107.50	21.07	81.98	20.35
(17,0)	111.12	22.13	120.40	23.47	91.57	22.63
(19,0)	134.43	26.75	147.15	28.61	112.14	27.57
(20,0)	148.89	29.63	161.99	31.39	123.20	30.22
(22,0)	175.71	34.96	192.98	37.30	147.01	35.88
(23,0)	191.83	38.25	209.82	40.46	159.59	38.89
(25,0)	222.06	44.30	245.09	47.15	186.67	45.29

FIGURE 4. CPKS transverse polarizabilities per unit length as a function of the radius in the three approaches LDA(L), LDA(V), and B3LYP(L). The three curves have been fitted by parabola type functions whose expressions are given in the captions. [Color figure can be viewed in the online issue, which is available at wileyonlinelibrary.com.]

calculated and they are almost the same as the CPKS ones. For example, for (10,0), at the LDA level, the calculated values are 9.19 and 9.45 Å^2 for the FF and CPKS methods, respectively. The CPKS values are very similar to the screened values previously published [16]. The LDA/CPKS results are higher by only 4% from the B3LYP/CPKS reference. This relatively small difference

found for α^{zz} with the two hamiltonian LDA and B3LYP operators proves that the transverse polarizability of SWCN does not depend on the bandgap when relaxation of the orbitals due to the field is taken into account. Contrarily to the longitudinal field, a strong and similar influence of the local field effects appears at the LDA and B3LYP level of calculation in this field direction, as can be seen by comparing SOS and CPKS values of the transverse component of the polarizability.

The $\alpha_0^{zz}/\alpha^{zz}$ screening factors computed with the length operator grow slowly as the radius increases (from 4.8 to 5.2 and from 3.7 to 4.1 at the LDA and B3LYP levels, respectively). As at present only the SOS approach allows to compute the frequency dependence of the polarizabilities from the CRYSTAL one electron approach, it is essential to correct the transverse component by taking into account the depolarization effect. The classical Clausius Mossotti relation [see relation (1)] can then be used but it is necessary to replace the radius of the carbon backbone by an effective radius $\tilde{R} = R + \delta R$ consistent with the finite thickness of the electronic charge density distribution. However, the question of what is the appropriate δR must be solved. Benedict and coworkers proposed to fix δR to 1.2 Å as for fullerenes to correct their RPA polarizabilities. On the other hand, Kozinsky and Marzari proposed to treat a nanotube as a dielectric cylindrical shell of finite thickness. They showed that the screened transverse

TABLE V _____

Transverse SOS polarizabilities per unit length (in Å^2) of the zigzag single walled carbon (m, 0) nanotubes with $m \neq 3n$ for $m = 7$–25 corrected to include the depolarization effect with the classical Clausius Mossotti relation. For the three approaches [LDA(V), LDA(L), B3LYP(L)], the values obtained with both δR = 1.2 Å and our optimised δR values are reported and compared to the reference CPKS values.

	LDA(V)			LDA(L)			B3LYP(L)		
	CPKS	1.2 Å	0.79 Å	CPKS	1.2 Å	0.84 Å	CPKS	1.2 Å	0.93 Å
(7,0)	4.95	5.94	5.03	5.38	6.10	5.27	5.24	5.68	5.13
(8,0)	6.33	7.35	6.30	6.66	7.47	6.53	6.47	6.96	6.34
(10,0)	8.75	10.20	8.96	9.45	10.42	9.31	9.18	9.75	9.01
(11,0)	10.47	11.97	10.61	11.10	12.17	10.96	10.75	11.39	10.58
(13,0)	13.64	15.61	14.05	14.69	15.92	14.53	14.22	14.93	13.99
(14,0)	15.74	17.75	16.08	16.71	18.05	16.56	16.15	16.92	15.92
(16,0)	19.64	22.14	20.27	21.07	22.58	20.90	20.35	21.19	20.07
(17,0)	22.13	24.60	22.62	23.47	25.03	23.26	22.63	23.49	22.31
(19,0)	26.75	29.80	27.61	28.61	30.38	28.42	27.57	28.54	27.22
(20,0)	29.63	32.62	30.32	31.39	33.21	31.16	30.22	31.19	29.82
(22,0)	34.96	38.56	36.06	37.30	39.33	37.10	35.88	36.98	35.47
(23,0)	38.25	41.74	39.14	40.46	42.54	40.21	38.89	39.99	38.42
(25,0)	44.30	48.43	45.62	47.15	49.44	46.92	45.29	46.51	44.81
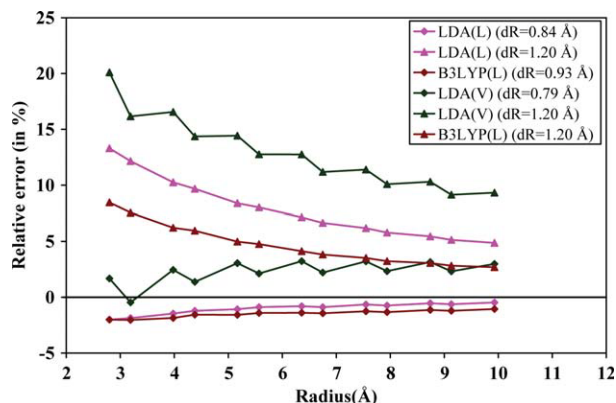
FIGURE 5. Relative errors (in %) between the corrected SOS and CPKS values (from the CPKS reference) of the transverse polarizabilities per unit length as a function of the SWCN radius (in Å). For each approach, we consider both our calculated δR values and $\delta R = 1.2$ Å, value used in previous articles to correct the SOS polarizabilities. [Color figure can be viewed in the online issue, which is available at wileyonlinelibrary.com.]

polarizability α^{zz} varies linearly with the square of the effective tube radius ($\alpha^{zz} = c\tilde{R}^2$ with $c < 1/2$ for semiconducting systems). We have applied this model to our CPKS data and performed least square fits on $\alpha^{zz} = f(R) = c(R+\delta R)^2$ (see Fig. 4 for the equation of the parabola) which yield very similar c slopes for the three CPKS approaches. (0.406, 0.386, 0.385 for LDA/L, LDA/V, and B3LYP/L, respectively) and allow to evaluate the radial extension δR, for each approach. Our δR values (0.84, 0.79, and 0.93 Å for LDA/L, LDA/V, and B3LYP/L, respectively) are found lower than the previously reported corrections (1.2 or 1.3 Å). We have then used these values in the Clausius-Mossotti equation to correct the unscreened transverse polarizabilities and obtained the results reported in Table V. As shown on Figure 5, the relative errors between the corrected SOS and CPKS values (from the CPKS reference) are reduced to less than 1.5% for the largest radii at both LDA and B3LYP levels. In the following step, we will restore the frequency dependence and apply the same correction on the dynamic transverse polarizabilities computed at the SOS level. In particular, the mean dynamic polarizability [$\alpha(\omega)$] allows to calculate the optical properties of the nanotubes, such as reflectivity and absorption via the complex dielectric function $\varepsilon(\omega) = 1 + 4\pi N\alpha(\omega)$ (where N is the number of moieties per volume unit).

4. Conclusion

We have used the CPKS method, which includes analytically the local field effects to compute both transverse and longitudinal polarizabilities of the (m, 0) SWCN series with $m \neq 3n$ for $m = 7$–25. As stated in previous studies, the comparison with SOS values obtained in the same computational conditions clearly confirms that the longitudinal polarizabilities are slightly sensitive to the polarization effect. On the other hand, the unscreened SOS tranverse polarizabilities which are found 4 to 5 time larger than the screened CPKS ones have been corrected to account for the local field effect. This correction based on the classical Clausius-Mossotti relation has be fitted on the CPKS values taken as reference, assuming a linear variation with the square of the effective tube radius. This trend available for tubes with relatively low radius cannot be extended to systems with large radii, which would imply an infinite transverse polarizability. This correction will be used to calculate the frequency dependent transverse dielectric function, which is directly related to the optical properties of the nanotubes.

References

1. Dean, K. A.; Chalamala, B. R. Appl Phys Lett 2000, 76, 375.
2. Tans, S. J.; Verschueren, A. R. M.; Dekker, C. Nature 1998, 393, 49.
3. Dai, H. Surf Sci 2002, 500, 218.
4. Benedict, L. X.; Louie, S. G.; Cohen, M. L. Phys Rev B: Condens Matter Mater Phys 1995, 52, 8541.
5. Liu, H. J.; Chan, C. T. Phys Rev B 2002, 66, 115416.
6. Guo, G. Y.; Chu, K. C.; Wang, D.-S.; Duan, C.-G. Comput Mat Sci 2004, 30, 269.
7. Zhou, X.; Chen, H.; Zhong-Can, O.-Y. J Phys: Condens Matter 2001, 13, L635.
8. O'Keeffe, J.; Wei, C.; Cho, K. App Phys Lett 2002, 80, 676.
9. Li, Y.; Rotkin, S. V.; Ravaioli, U. Nano Lett 2003, 3, 183.
10. van Faasssen, M.; Jensen, L.; Berger, J. A.; de Boeji, P. L. Chem Phys Lett 2004, 395, 274.
11. Jensen, L.; Åstrand, P.-O.; Mikkelsen, K. V. Nano Lett 2003, 3, 661.
12. Kozinsky, B.; Marzari, N. Phys Rev Lett 2006, 96, 166801.
13. Jensen, L.; Esbensen, A. L.; Åstrand, P.-O.; Mikkelsen, K. V. J Comput Methods Sci Eng 2006, 6, 353.
14. Mayer, A. Phys Rev B: Condens Matter Mater Phys 2007, 75, 045407.
15. Sebastiani, D.; Kudin, K. N. ACS Nano 2008, 2, 661.

16. Brothers, E. N.; Kudin, K. N.; Scuseria, G. E.; Bauschlicher, C. W. Phys Rev B: Condens Matter Mater Phys 2005, 72, 33402.

17. Brothers, E. N.; Kudin, K. N.; Scuseria, G. E. J Chem Phys 2006, 124, 041101.

18. Brothers, E. N.; Kudin, K. N.; Scuseria, G. E. J Phys Chem B 2006, 110, 12860.

19. Brothers, E. N.; Izmaylov, A. F.; Scuseria, G. E.; Kudin, K. N. J Phys Chem C 2008, 112, 1396.

20. Guo, G. Y.; Chu, K. C. Phys Rev 2004, 69, 205416.

21. Machon, M.; Reich, S.; Thomsen, C.; Sanchez-Portal, D.; Ordejon, P. Phys Rev B 2002, 66, 155410.

22. Arab, M.; Picaud, F.; Devel, M.; Ramseyer, C.; Girardet, C. Phys Rev B 2004, 69, 165401.

23. Langlet, R.; Arab, M.; Picaud, F.; Devel, M.; Girardet, C. J Chem Phys 2004, 121, 9655.

24. Baraille, I.; Rérat, M.; Mora, P. Phys Rev B 2006, 73, 075410.

25. Casimir, H. B. G.; Polder, D. Phys Rev 1948, 73, 360.

26. Ferrero, M.; Rérat, M.; Orlando, R.; Dovesi, R. J Comp Chem 2008, 29, 1450.

27. Ferrero, M.; Rérat, M.; Orlando, R.; Dovesi, R.; Bush, I. J. J Phys Conf Series 2008, 117, 12016.

28. Saunders, V. R.; Dovesi, R.; Roetti, C.; Orlando, R.; Zicovich-Wilson, C. M.; Pascale, F.; Harrison, N. M.; Doll, K.; Civalleri, B.; Bush, I. J.; D'Arco, P.; Llunell, M.; In CRYSTAL06 User's Manual University of Torino: Torino, 2006.

29. Frey, J. T.; Doren, D. J. TubeGen 3.3, University of Delaware, Newark DE, Available at: http://turin.nss.udel.edu/research/tubegenonline.html, 2005. Accessed on February 15, 2010.

30. Dovesi, R.; Civalleri, R.; Orlando, R.; Roetti, C.; Saunders, V. R. Reviews in Computational Chemistry, Chapter 1, Volume 21; John Wiley & Sons, Inc.: New York, 2005; Available at: http://www.crystal.unito.it. Accessed on February 20, 2010.

31. Dirac, P.A.M. Proc Cambridge Phil Soc 1930, 26, 376.

32. Vosko, S. H.; Wilk, L.; Nusair, M. Can J Phys 1980, 58, 1200.

33. Becke, A. D. J Chem Phys 1993, 98, 5648.

34. Lee, C.; Yang, W.; Parr, R. G. Phys Rev B 1988, 37, 785.

35. Resta, R.; Kunc, K. Phys Rev B 1986, 34, 7146.

36. Darrigan, C.; Rérat, M.; Mallia, G.; Dovesi, R. J Comp Chem 2003, 24, 1305.

37. Gajdos, M.; Hummer, K.; Kresse, G.; Furthmüller, J.; Bechstedt, F. Phys Rev B 2006, 73, 45112.

38. Rérat, M.; Ferrero, M.; Amzallag, E.; Baraille, I.; Dovesi, R. J Phys Conf Series 2008, 117, 012023.

39. Pandey, R.; Rérat, M.; Causà, M. Appl Phys Lett 1999, 75, 4127.

40. Pandey, R.; Rérat, M.; Darrigan, C.; Causà, M. J Appl Phys 2000, 88, 6462.

41. He, H.; Orlando, R.; Blanco, M. A.; Pandey, R.; Amzallag, E.; Baraille, I.; Rérat, M. Phys Rev B 2006, 74, 195123.

42. Groh, D.; Pandey, R.; Sahariah, M. B.; Amzallag, E.; Baraille, I.; Rérat, M. J Phys Chem Solids 2009, 70, 798.

43. Adolph, B.; Gavrilenko, V. I.; Tenelsen, K.; Bechstedt, F.; Del Sole, R. Phys Rev B 1996, 53, 9797.

44. Weisman, R. B.; Bachilo, S. M. Nano Lett 2003, 3, 1235.

45. Jespersen, T. S. Raman Scattering in Carbon Nanotubes, Master thesis, Niels Bohr Institute, Copenhagen University; Denmark, 2003.

46. Muscat, J.; Wander, A.; Harrison, N. M. Chem Phys Lett 2001, 342, 397.